HHS Public Access

Author manuscript

*Neuroimage*. Author manuscript; available in PMC 2018 August 22.

Published in final edited form as:

*Neuroimage*. 2017 July 15; 155: 147–158. doi:10.1016/j.neuroimage.2017.04.067.

# High-resolution Functional MRI Identified Distinct Global Intrinsic Functional Networks of Nociceptive Posterior Insula and S2 regions in Squirrel Monkey Brain

**Ruiqi Wu**[1,2,4], **Feng Wang**[1,2], **Pai-Feng Yang**[1,2], and **Li Min Chen**[1,2,3,*]

[1)]Institute of Imaging Science, Vanderbilt University, Nashville, Tennessee 37232

[2)]Department of Radiology and Radiological Sciences, Vanderbilt University Medical Center, Nashville, Tennessee 37232

[3)]Department of Psychology, Vanderbilt University, Nashville, Tennessee 37232

[4)]Wuhan Institute of Physics and Mathematics, The Chinese Academy of Sciences/State Key Laboratory of Magnetic Resonance and Atomic and Molecular Physics, Wuhan, China 430071,

## Abstract

Numerous functional imaging and electrophysiological studies in humans and animals indicate that the two contiguous areas of secondary somatosensory cortex (S2) and posterior insula (pIns) are core regions in nociceptive processing and pain perception. In this study, we tested the hypothesis that the S2-pIns connection serves as a hub for connecting distinct sensory and affective nociceptive processing networks in the squirrel monkey brain. At 9.4T, we first mapped the brain regions that respond to nociceptive heat stimuli with high-resolution fMRI, and then used seed-based resting-state fMRI (rsfMRI) analysis to delineate and refine the global intrinsic functional connectivity circuits of the proximal S2 and pIns regions. In each subject, nociceptive (47.5 °C) heat-evoked fMRI activations were detected in many brain regions, including primary somatosensory (S1), S2, pIns, area 7b, anterior cingulate cortex (ACC), primary motor cortex (M1), prefrontal cortex (PF), supplementary motor area (SMA), thalamus, and caudate. Using the heat-evoked fMRI activation foci in S2 and pIns as the seeds, voxel-wise whole-brain resting-state functional connectivity (rsFC) analysis revealed strong functional connections between contralateral S2 and pIns, as well as their corresponding regions in the ipsilateral hemisphere. Spatial similarity and overlap analysis identified each region as part of two distinct intrinsic functional networks with 7% overlap: sensory S2-S1-area 7b and affective pIns-ACC-PCC networks. Moreover, a high degree of overlap was observed between the combined rsFC maps of nociceptive S2 and pIns regions and the nociceptive heat-evoked activation map. In summary, our study provides evidence for the existence of two distinct intrinsic functional networks for S2 and pIns nociceptive regions, and these two networks are joined via the S2-pIns connection. Brain regions that are involved in processing nociceptive inputs are also highly interconnected at rest. The presence of robust and distinct S1-S2-area 7b and pIns-ACC-PCC rsFC networks under anesthesia underscores their fundamental roles in processing nociceptive information.

[*]**Corresponding author:** Li Min Chen MD, PhD, Associate Professor, Department of Radiology and Radiological Sciences, Institute of Imaging Science, Vanderbilt University Medical Center, 1161 21st Ave. S., AA 1105 MCN, Nashville, TN 37232-2310, Tel: 615 9367069, 615 3220734, limin.chen@vanderbilt.edu.

**Keywords**

resting-state functional connectivity; whole brain; pain; posterior insula; the secondary somatosensory cortex; monkey

## 1. Introduction

With data from three decades of functional studies (including fMRI, PET, EEG, and MEG) in humans, it is now commonly accepted that the complex and multi-dimensional experience of pain is represented by coordinated activities of multiple cortical regions, including primary somatosensory cortex (S1), secondary somatosensory cortex (S2), primary motor cortex (M1), insula cortex, thalamus, anterior cingulate cortex (ACC), and prefrontal cortex (PF) (Apkarian et al., 2005; Bornhovd et al., 2002; Casey, 1999; Chen, 2001; Haefeli et al., 2014; Kwan et al., 2000; Peyron et al., 2000). What remains elusive is how these different brain regions interact to generate this complex pain experience. Advanced MRI studies of patients in various chronic pain conditions have led to exciting discoveries of profound anatomical and functional abnormalities in many of these brain regions, either as individual areas or as part of a network (i.e., connections between regions), which supports the idea that dysfunctions of different brain networks contribute to chronic pain symptoms (Apkarian et al., 2005; Apkarian et al., 2001; May, 2008; Napadow et al., 2010). Many research efforts have now been devoted to exploring abnormality of functional connectivity within and across different brain networks (e.g., sensorimotor or default mode network) in chronic pain conditions using resting state fMRI (rsfMRI) signals (Baliki et al., 2008; Davis and Moayedi, 2013; Malinen et al., 2010; Napadow et al., 2010).

To date, rsfMRI has become a predominant method for identifying and parcellating intrinsic functional connectivity networks (Fox and Greicius, 2010; Greicius et al., 2003; van den Heuvel and Pol, 2010). To facilitate clinical chronic pain research and help interpret rsfMRI findings, it is necessary to first parcellate and refine intrinsic functional connectivity networks of the normal pain system, and then to explore the underlying neural electrophysiological basis of rsfMRI signals. RsfMRI defines the functional connectivity at resting-state (rsFC) by quantifying the temporal correlation between spatially remote brain regions when the subject is not performing an explicit task (Biswal et al., 1995). Animal studies, particularly those using non-human primates and invasive procedures, have provided strong evidence validating the use of rsfMRI signals in probing inter-regional neural functional connectivity (Hutchison et al., 2013; Margulies et al., 2009; Scholvinck et al., 2010; Vincent et al., 2007; Wang et al., 2013). For example, our group and others have shown that S1 and visual cortices of monkeys display synchronized fluctuations of rsfMRI signals with other brain regions, which have been shown to correlate closely with fluctuations in spontaneous local field potentials or spiking activity in an anatomically constrained manner (Shmuel and Leopold, 2008; Wang et al., 2013). Building upon these advances, the present study aims to parcellate the whole-brain intrinsic functional connectivity networks of nociceptive systems of monkeys, with a primary focus on S2 and posterior insula (pIns) regions that reside along the upper bank of the lateral sulcus in

monkeys (i.e., the homologous region with the operculoinsular along the *Sylvian fissure* of the human brain).

We focused this study on the intrinsic functional circuits of S2 and pIns. It has been technically challenging to define and separate these two regions with high confidence in human fMRI studies, due mainly to their close spatial proximity in conjunction with the imaging resolution typically employed in these studies (Garcia-Larrea et al., 2003; Sawamoto et al., 2000; Vogel et al., 2003). In many of the pain imaging studies, the S2 (part of parietal operculum) and pIns are not readily separable, and are often considered a single functional entity (Garcia-Larrea et al., 2003; Iannetti et al., 2005; Peyron et al., 2002; Vogel et al., 2003). The uncertainty in localizing pain-related regions in the operculoinsular region, along with the lack of refined functional connectivity networks of nociceptive S2 and pIns regions, motivated us to conduct a similar study in monkeys. Thus, in this study, we first defined nociceptive regions with noxious heat stimulation, and then parcellated functional networks using rsfMRI signals on an individual subject basis. We also performed cluster tree analysis to determine the hierarchical organization of the rsFC networks. We identified two distinct intrinsic functional networks for S2 and pIns nociceptive regions, and found close relationships between the nociceptive processing network and rsFCs of these two regions.

## 2. Methods and Materials

### 2.1. Animal preparation

Four adult male squirrel monkeys (*Saimiri sciureus*) were included in this study. For the fMRI experiments, animals were initially sedated with ketamine hydrochloride (10 mg/kg) and atropine sulfate (0.05 mg/kg), and then anesthetized with isoflurane (0.7%−1.2%) delivered in a 70:30 $N_2O/O_2$ mixture. After intubation, the animal was placed in custom-designed MR cradle with the head secured by ear bars and head bars. During functional MRI data acquisition, animals were maintained at a light (0.5–0.8%) and stable level of anesthesia. A solution of 2.5% dextrose in saline solution was infused intravenously (3 ml/kg/h) to prevent dehydration. Animals were artificially ventilated to maintain an end-tidal $CO_2$ of 4%. Rectal temperature was maintained (SA Instruments) between 37.5 °C and 38.5 °C by means of a circulating water blanket. Heart rate and peripheral capillary oxygen saturation (SpO2; Nonin), respiration pattern and EKG (SA Instruments), and end-tidal $CO_2$ (22–26 mmHg; SurgiVet) were continuously monitored during the entire procedure. In 90% of our imaging runs, the heart rate was stable, with changes < 10 bpm during the stimulation. SpO2 was usually very stable, as well, staying at >95% during the entire experiment. All procedures were conducted in accordance with National Institutes of Health and ARRIVE guidelines, and were approved by the Institutional Animal Care and Use Committee of Vanderbilt University.

### 2.2. Stimulation protocol

The fingers were stabilized with modeling clay, palm side up, leaving the glabrous skin of the distal finger pads available for stimulation. Noxious heat stimuli were presented on distal finger pads of D2 and D3 (right hands in three monkeys, and left hand in one monkey), and delivered via a CHEPS thermal probe with rapid heating rate of 70°C/s (Medoc Advanced

Medical Systems). For each fMRI noxious heat (47.5 °C) stimulation run, 21 sec duration blocks of 47.5 °C heat were repeated nine times with 30 sec baseline (32 °C) periods in between.

### 2.3. MRI data acquisition and analyses

All MRI scans were performed on a 9.4 T 21 cm narrow-bore MRI scanner (Varian Medical Systems) using a quadrature birdcage volume coil (inner diameter = 85mm, Doty 85) centered over the brain. A series of T2*-weighted multi-slice gradient echo high-resolution structural axial images (TE = 10 ms, TR = 500 ms, 0.125 × 0.125 × 1 $mm^3$ voxel size, 512 × 512 × 28 matrix) were collected. FMRI data were acquired from the same slices using a two-shot gradient echo planar imaging (GE-EPI) sequence (TE = 16 ms, TR = 1.5 sec, 1 × 1 × 1 $mm^3$ voxel size, 64 × 64 × 28 matrix, interleaved slices, linear K space filling, 3s/volume). An extra navigator echo was collected with no phase encoding prior to acquisition of the actual image data. This echo is used to correct for phase variations typically caused by motion. FMRI data with and without heat stimulation were collected with the same functional imaging acquisition parameters. In a typical fMRI session (day), 8 to 12 stimulation and 3 to 4 resting-state runs (170 volumes per run) were acquired. A total of five imaging sessions were performed (one monkey underwent two imaging sessions). Specifically, 12, 5, 8, 9, and 1 stimulation runs and 4, 3, 4, 3, and 1 rsfMRI runs were acquired from Monkey SM-HAZ (sessions 1 and 2), SM-GAL, SM-SUL, and SM-SUP, respectively.

Functional EPI data (stimulus and resting-state) were pre-processed with slice timing and head motion correction (3dTshift, AFNI), and physiological noise correction using RETROICOR algorithm (3dretroicor, AFNI) (Glover et al., 2000). For image quality control, datasets with motion artifacts of head rotation > 0.3 degree or/and head translation > 0.2 mm (1/5 voxel size) were excluded from the subsequent analyses and quantification. To preserve the highest resolution possible, no spatial smoothing was applied. The stimulus-evoked EPI data were temporally smoothed with a low-pass filter with a 0.25 Hz cutoff frequency, and the rsfMRI data with a 0.1 Hz cutoff frequency (3dFourier, AFNI). Activation maps were created by voxel-wise analysis, using the Hemodynamic Response Function (HRF) convolved with the stimulus presentation paradigm (3dDeconvolve, AFNI). Activation map (FDR corrected, $p < 0.05$) was generated for each run. Group (multiple runs) activation maps were created by t-test performed on β value of each run across multiple runs (typically 8–12 runs) obtained within the same imaging session, and then displayed as statistical *t*-value maps (with a threshold of *t*-value = 2, $p < 0.05$). BOLD fMRI signal time courses were extracted from a peak voxel in each area of S2 and pIns to quantify the amplitudes of BOLD responses to stimuli in each run, and then averaged across multiple runs and across animals. EPI data were up-sampled from 64 × 64 × 28 to 128 × 128 × 28 matrix, and co-registered on corresponding T2-weighted high-resolution anatomical images using a linear image registration tool (flirt, FSL) for display.

Seed-based rsfMRI analysis was performed to determine the intrinsic functional connectivity network of nociceptive S2 and pIns regions in each animal. The activations were identified by overlaying the group heat-evoked activation map on three reconstructed image planes

(sagittal, axial, and coronal) generated from multiple runs on the anatomical MR image of the same subject, while referencing the histology sections (http://neurosciencelibrary.org/specimens/primates/squirrelmonk/), atlas, and anatomical papers of squirrel and macaque monkeys (Gergen and MacLean, 1962; Jones and Burton, 1976; Saleem and Logothetis, 2012). The selections of S2 and pIns seeds were based upon different local maxima (i.e., voxels showing strongest responses to nociceptive stimuli) within each of the anatomically defined S2 and pIns regions. Each correlation coefficient (r value indicating the strength of rsFC) map was generated using one to two voxels as a seed. Whole brain voxel-wise correlation analysis was performed (3dfim, AFNI) by using filtered rsfMRI signals extracted from S2 and pIns seeds as the predictors for each run. Multiple-run averaged group correlation coefficient maps of S2 or pIns seeds were calculated and displayed (threshold *r*-value > 0.2, $p < 0.05$) with warm color indicating high correlation value (e.g., Fig. 2A&B). For illustration purposes, only image slices with significant activations and correlation foci were displayed. The hemisphere on the same side as the stimulation was defined as the ipsilateral hemisphere, while the opposite was labeled as the contralateral one.

### 2.4. Similarity analysis of the functional connectivity pattern

To quantify the relationship or similarity between activation map and rsFC networks, two analyses (i.e., spatial correlation coefficient (SCC), and overlap percentage) were performed. For both SCC and overlap percentage calculations, only multi-run group rsFC maps (thresholded at $r > 0.2$) and activation maps (thresholded at $t > 2$) were used. Four pairs of maps from the same session were compared to determine the relationships between: S2 and pIns rsFC maps (rS2|rpin, n = 30 pairs), S2 rsFC and activation map (rS2|activ, n = 10 pairs), pIns rsFC map and activation map (rpin|activ, n = 12 pairs), and combined S2-pIns intrinsic map and activation map (comb|active, n = 30 pairs). Combined rsFC map of S2 and pIns (comb) was derived by linearly conjoining of two rsFC maps. We typically chose 2–3 seeds at or around the activation peaks of S2 and pIns for deriving rsFC maps. Only the sessions with more than 3 runs were included in the SCC and overlap percentage analysis. One subject (SM-SUP) was excluded in the analysis, because only one resting-state and one stimulation runs were acquired. In total, rsFC maps of ten S2 and twelve pIns seeds from three subjects were included in the quantification (SM-GAL: 3 S2 and 3 pIns seeds, SM-SUL: 3 S2 and 3 pIns seeds, SM-HAZ session 1: 2 S2 and 3 pIns seeds, and SM-HAZ session 2: 2 S2 and 3 pIns seeds).

The method of generating SCC values was adopted from published studies (Ramsden et al., 2001; Xu et al., 2003). Briefly, SCC values are computed on a voxel-by-voxel basis by converting activation and correlation coefficient maps into binary format maps in which the value of a single voxel is either 1 (above threshold) or 0 (below threshold). In a comparison of two different maps, a given voxel must belong to one of the four categories: [1,1], [1,0], [0,1], and [0,0]. $N_{[1,1]}$, $N_{[1,0]}$, $N_{[0,1]}$, and $N_{[0,0]}$ are the total numbers of the voxel in the corresponding categories. When $N_{[1,1]}*N_{[0,0]} > N_{[1,1]}*N_{[1,0]}$, SCC is mathematically defined as (Cole et al.,1949):

$$SCC = \frac{N[1,1]N[0,0] - N[1,0]N[0,1]}{(N[1,0] + N[1,1])(N[1,0] + N[0,0])}$$

The absolute values of the SCC tracks with the $\chi^2$ statistic, and SCC values greater than 0.15 are highly significant ($p < 0.001$) with the number of voxels in the maps used for this study. To measure the overlap percentage of two different maps, one map was overlaid onto another, and the percentage of voxels presented in both maps over those presented in either map separately was calculated. The range of overlap percentage between two maps is from 0 to 1. SCC and overlap percentage results are presented as mean ± standard error (SE) (Fig. 4). Unpaired t-tests were performed to compare the SCC and overlap percentage differences between different maps. A *p*-value below 0.05 was considered statistically significant.

### 2.5. Inter-regional correlation and hierarchical cluster analysis

To investigate the relationships between different regions within S2 and pIns rsFC networks, inter-regional correlations were then calculated. Twelve regions (ipsilateral and contralateral ACC (iACC, cACC), posterior cingulate cortex (iPCC, cPCC), pIns (ipIns, cpIns), area 7b (i7b, c7b), S2 (iS2, cS2), and S1 (iS1, cS1)) that showed the most consistent and reproducible activation to nociceptive heat stimuli and rsFC to S2 or pIns regions were chosen for inter-regional correlation coefficient analysis. Specifically, Pearson correlations among the twelve main cortical regions within these two networks were calculated on a single-voxel basis. A 12 × 12 region-region correlation matrix was generated using the highest correlation coefficient value of each specific region-region pair. Averaged inter-regional correlation coefficients (r-values) with their corresponding standard error (SE) was calculated across all of the 15 rsfMRI runs from 4 animals and 5 sessions, and are presented as matrix plots in Fig. 5.

We lastly investigated the hierarchical relationship among all cortical regions of the two intrinsic nociceptive networks by using a hierarchical clustering method (Edelbrock and McLaughlin, 1980; Johnson, 1967). Clustering was based on time courses of different regions, and was determined using the correlation metric and weighted average linkage (WPGMA) clustering criterion. Dendrogram plots of the hierarchical binary cluster trees were generated among three groups of regions: all twelve regions, ten regions excluding the bilateral pIns, and ten regions excluding bilateral S2 (Fig. 5C). On the tree graph, the length of each U-shaped line represents the distance between the connected regions.

## 3. Results

### 3.1. Nociceptive heat-evoked fMRI responses

Nociceptive heat-evoked fMRI responses were first investigated in the whole brain of squirrel monkeys. Heat (47.5 °C) stimulation of D2 and D3 of the right hand evoked robust and wide-spread fMRI activations in many cortical regions, including bilateral area 3a/3b and area 1/2 of S1 (slices 5–6, 10–11), bilateral S2 (slices 10–14), bilateral pIns (pin, slice 14), bilateral posterior parietal cortex (Pari, slices 8–10), ipsilateral auditory cortex (Aud, slices 11–12), ipsilateral primary motor cortex (M1, slice 2), ACC (slices 7–9), pre-supplementary motor area (preSMA, slice 5), supplementary motor area (SMA, slice 5), caudate (slice 13), thalamus (slice 18), and prefrontal cortex (PF, slice 8) (Fig. 1A). Stimulus-evoked BOLD signal changes were exacted from each activated region, and the peak signal changes ranged from 0.19% ± 0.03% to 0.37% ± 0.03% (Fig. 1B). The strongest

response was observed in ipsilateral area 7b (i7b), whereas the weakest response was observed in contralateral pIns (cpin). Even though the S2 and pIns activation foci are located in very close proximity, they are apparently separable (see the two peak foci in the insert of slice 14). To observe these two foci more clearly, a smoothed mesh and contour plot of the activation was presented in Fig. 1C. Mean BOLD time courses extracted from S2 and pIns regions showed robust stimulus-evoked signal changes (Fig. 1D, red line indicates S2 and blue line indicates pIns). Voxels around the heat-evoked S2 and pIns fMRI activation foci (black squares within orange outline in Fig. 1C left image) were used as the seeds in the next step of the voxel-wise whole-brain rsFC analysis. The composite map (right image in Fig. 1C) shows the spatial relationship of the selected S2 and pIns seeds, along with the corresponding anatomical territories of S2 and pIns regions, as defined by the atlas (see the orange and light blue patches in Fig. 1C right image).

### 3.2. Distinct intrinsic rsFC maps of nociceptive S2 and pIns regions

Seed-based whole-brain voxel-wise correlation analysis revealed two distinct rsFC networks of S2 and pIns regions that were responsive to nociceptive heat stimuli. We found that the contralateral S2 seed (slice 14, Fig. 2A) in the same representative subject shown in Fig. 1 exhibited robust local functional connectivity to ipsilateral S2 (slices 12–15), bilateral area 3a/3b and area 1/2 of S1 (slices 12–14), bilateral area 7b (slice 5), bilateral pIns (slices 13–14), and bilateral Pari (slices 8–9), with moderate connectivity to ACC (slices 8–9) (Fig. 2A). In contrast, the contralateral pIns seed (slice 14, Fig. 2B) showed strong connectivity to ipsilateral pIns (slices 15–16), bilateral Pari (slices 8–9), ACC (slices 8–10), and PCC (slices 9–10), as well as moderate connectivity to bilateral S2 (slice 14), bilateral area 7b (slice 6, 8), PF (slice 6), contralateral M1 (slices 4–6) and Aud (slice 14) (Fig. 2B). The enlarged views of the local correlation patterns in S2 and pIns regions illustrate their close but separated local correlation profiles in S2-rsFC (Fig. 2C right) and pIns-rsFC maps (Fig. 2D left). Smoothed mesh and contour plots of the S2 and pIns *r*-value distributions also show S2 and pIns are apparently separable in both S2- (Fig. 2C) and pIns-rsFC maps (Fig. 2D).

Similar rsFC patterns were observed in the other three monkeys; two cases are presented in Fig. 3. The same method was used to identify the S2 and pIns seeds (Fig. 3A & 3D). Again, strong connectivity of the S2 seed to ipsilateral S2, bilateral S1, bilateral 7b, and bilateral pIns were observed in both monkeys (SM-HAZ: Fig. 3B; and SM-GAL: Fig. 3E). Strong connectivity of the pIns seed was detected among ipsilateral pIns, bilateral S2, area 7b, and ACC (SM-HAZ: Fig. 3C; SM-GAL: Fig. 3F). The intrinsic networks of S2 and pIns identified in these two subjects were similar to the case presented in Fig. 2.

Interestingly, most of the regions showing strong rsFC to S2 and pIns heat nociceptive regions (i.e., bilateral S2, bilateral pIns, bilateral S1, bilateral area 7b, and ACC) also showed strong responses to nociceptive stimulation (compare Fig. 1A with Fig. 2). The presence of nociceptive-stimulus responsive M1, thalamus, and FC regions within the S2 and pIns rsFC networks was more variable, and was only detected in the pIns rsFC network in one monkey (SM-HAZ, Fig. 2B). Thus, these three regions were excluded in the next step of similarity analysis.

### 3.3. Similarity between nociceptive heat-evoked activation map, S2 and pIns intrinsic rsFC networks

We conducted SCC analysis to examine the extent to which the three different maps (or networks) of rsFC of nociceptive S2 and pIns regions overlap or differ from each other, and how each compares to the nociceptive heat activation map. It is notable that many of the regions were identified repeatedly in these three networks, but the overall rsFC patterns of the S2 and pIns seeds looked quite different. Therefore, SCC and overlap percentage were calculated to quantify similarities between different functional maps (networks) (Fig. 4). High SCC values indicate high similarity between two maps. First, we found that the SCC value between S2 and pIns rsFC maps was small (SCC = 0.106 ± 0.010), indicating low similarity between these two rsFC networks (left column in Fig. 4A). In contrast, the SCC values of rS2|active (SCC = 0.293 ± 0.073), rpin|active (SCC = 0.209 ± 0.030), and comb|activ (SCC = 0.199 ± 0.014) were greater than 0.15 (Fig. 4A), which were highly significant ($p < 0.001$, the SCC values tracks with the $\chi^2$ statistic). SCC value was the highest between the heat activation and S2 rsFC maps. However, there were not significant differences between the heat activation map and S2 (rS2/active), pIns (rpin|active), or combined (comb|active) rsFC maps (the right three columns in Fig. 4A). Importantly, the SCC values of these three pairs (rS2|active ($p = 1.28 \times 10^{-5}$), rpin|active ($p = 9.55 \times 10^{-5}$), and comb|activ ($p = 5.92 \times 10^{-7}$)) were significantly higher than that of rS2|rpin (unpaired t-test, Fig. 4A). These observations indicate that there were significant similarities (or comparability) between the heat-evoked activity map and the three rsFC maps.

The overlap percentage was 7.2 ± 0.6% for rS2|rpin, 9.0 ± 0.7% for rS2|active, 7.2 ± 0.9% for rpin|active, and 12.7 ± 0.4% comb|active. However, the overlap of the comb|active was significantly higher than those of rS2|rpin ($p = 1.02 \times 10^{-11}$), rS2|active ($p = 6.05 \times 10^{-5}$), and rpin|active ($p = 2.17 \times 10^{-8}$, unpaired t-test, Fig. 4B). This significantly increased overlap of the comb|active indicates that the shared overlap region among all three maps is small/partial, or the individual networks are more independent, so additions of independent networks of S2-rsFC (rS2) or pIns-rsFC (rpin) increases the overlap. Together, these results show that the rsFC maps of S2 and pIns heat nociceptive regions showed high similarities with the heat-evoked activity map, and the combined rsFC map of S2 and pIns overlapped markedly with the activity map.

### 3.4. Hierarchical organization of regions within rsFC networks of nociceptive S2 and pIns

To determine whether and to what extent nociceptive S2 and pIns regions belong to different functional cortical networks, we performed pair-wise inter-regional rsFC and hierarchical cluster tree analyses between all possible pairs of the ROIs that exhibited either strong fMRI response to nociceptive-heat stimuli or strong rsFC to either or both nociceptive S2 and pIns regions, including bilateral S2, bilateral pIns, bilateral area 3a/3b, bilateral area 7b, bilateral ACC, and bilateral PCC. The 12 × 12 matrix plot of the group averaged inter-regional correlation coefficients ($r$-values) showed a fixed pattern of strong rsFC among subgroups of regions (see each group outlined by dotted red lines in Fig. 5A). Three main clusters are identified within the matrix. The strongest connections were observed between bilateral ACC, and between bilateral PCC (dark red patches between iACC-cACC, and between iPCC-cPCC in Fig. 5A). The second strongest connections were found between pIns and S2

seed regions in the same hemisphere (orange patch between iS2-ipin, and yellow patch between cS2-cpin in Fig. 5A). The third strongest connections were identified between bilateral pIns, area 7b, and S2 regions (green patches in Fig. 5A), indicating strong inter-hemispheric connections. Bilateral area 3a/3b also exhibited strong connectivity (see blue-green patches in Fig. 5A). The functional connectivity between ACC and PCC was moderate (light blue patches in Fig. 5A). The corresponding matrix plot of the standard errors of the inter-regional correlation matrix was presented in Fig. 5B, and showed very little across-region variations.

For hierarchical cluster tree analysis, the WPGMA distance measure was derived to rank the strength of the inter-regional rsFC. The dendrogram plots of all twelve regions (Fig. 5C, left) showed that the distances between bilateral ACC and between bilateral PCC were shortest, and then between ipsilateral S2 and pIns, between contralateral S2 and pIns, between bilateral 7b, and then between bilateral area 3a/3b. To separate the potential influences of S2 and pIns seeds on each other's whole-brain network, we performed an additional analysis where either the S2 or pIns seed was excluded. Bilateral S2, bilateral area 3a/3b, and bilateral area 7b regions were clustered (strongly connected) when bilateral pIns were not in the network (Fig. 5C, middle). Bilateral pIns, ACC, and PCC were clustered when bilateral S2 were not in the network (Fig. 5C, right).

Together, the connection between ipsilateral S2 and pIns was the strongest. Two separate rsFC networks of pIns-ACC-PCC and S2-S1–7b were identified. These two networks were joined together by the S2 and pIns connection. Fig. 6 illustrates these two different functional networks (Fig. 6A) and their relationship (Fig. 6C).

## 4. Discussion

### 4.1. Refined nociceptive information process networks in non-human primate brain

The motivation to study nociception in non-human primates lies in their close resemblance to humans regarding brain structure and functions, as well as the fact that determination of their brain regions is based on multifactorial features, including cytoarchitectonic characteristics, neuronal response and receptive field properties, and anatomical connections. Availability of ultra-high MRI field permits fine-scale mapping of nociceptive processing regions and functional networks by simultaneously mapping and localizing pain (or non-pain) related activities throughout the entire brain at millimeter resolution within a single imaging session. This data acquisition strategy eliminates the imaging alignment errors, therefore drastically increasing the spatial precision for localizing stimulus-evoked brain responses and identifying seeds. As a demonstration of the effectiveness of our approach, we have detected nociceptive heat stimuli-evoked fMRI responses in S1 (areas 3a/3b and 1/2), S2, posterior insula (pIns), M1, SMA, ACC, dorsal PF cortices, thalamus (medial-dorsal and ventral-lateral nuclei), caudate, and amygdala in squirrel monkey brains under light anesthesia. Among these regions, fMRI responses in amygdala were relatively weaker and more variable across runs and animals. These findings are generally consistent with those reported in human fMRI studies (Bornhovd et al., 2002; Frot et al., 2013; Kwan et al., 2000; Oshiro et al., 2007; Peyron et al., 2000), as well as our previous fMRI stuides of the central and lateral sulci in monkeys (Chen et al., 2011; Chen et al., 2012). Taking one

step further, we are able to localize nociceptive heat stimuli-evoked responses to bilateral area 7b and posterior parietal cortices. Fairly robust activation was also detected in auditory cortex. We attribute this response to the activation in pIns, since pIns is known to participate multi-sensory functions and may have connections to the auditory cortices (Bamiou et al., 2003; Renier et al., 2009; Rodgers et al., 2008). Motor (and supplementary motor) activation is commonly observed in awake humans (Apkarian et al., 2005; Baliki et al., 2009; Peyron et al., 2000; Price., 2000) and anesthetized animals (Chen et al 2011) during painful stimulation. We interpret the motor activation via direct connections between M1 and S1 cortices (Pavlides et al., 1993; Petrof et al., 2015). The response could relate to the suppressive effect from S1 or other sensory cortices. However, fMRI signals are not capable of differentiating excitatory and inhibitory activity, because both activities increase energy consumption that leads to fMRI signal increases. One note is that our experimental setting of digit stimulation makes it hard to localize fMRI activation to S2 or PV (parietal ventral) sub-regions within the traditionally defined secondary somatosensory cortex (S2) without detailed electrophysiological map. Digits are presented as digit-to-digit somatotopic organization at the border of S2-PV (Coq et al., 2004), so digit stimulation-evoked fMRI activations merge together. Thus, here we use S2 to indicate the S2/PV region.

These findings are significant. First, the detection of nociceptive fMRI responses under light anesthesia in widely distributed brain regions beyond the sensorimotor cortices, particularly in high order PF and ACC, indicates that these brain regions are engaged in nociceptive processing (or at least showed nociceptive stimulus-related fMRI signal changes) without consciousness. Indeed, pain-avoidance neurons have been identified in the ACC of monkeys (Koyama et al., 2001; Koyama et al., 1998). Second, detection of robust and consistent heat-evoked fMRI activation in multiple closely localized lateral sulcus areas (i.e., S2, area 7b, and pIns) further supports the critical role of this S2-pIns circuit, which is homologous with the operculum-posterior insula region in the human brain, in nociception in primates. Nociceptive neurons, nociceptive heat-evoked field potential changes, and fMRI signals have been observed in monkey brain area 7b, pIns, and surrounding S2 (Chen et al., 2012; Chudler et al., 1986; Dong et al., 1994; Dong et al., 1996, for a review see Treede et al., 2000). Certainly, further investigations of neuronal activity and anatomical connection with invasive means in these regions are needed to fully appreciate the specific roles of these regions in individual processing, as well as processing as part of a functional network.

### 4.2. Two distinct intrinsic pain-related functional networks joint via S2-pIns connection

We focused this first study in S2-pIns region for two main reasons. First, S2 and pIns are central regions in pain perception. For example, both regions (also termed the operculoinsular region along the *Sylvian fissure* in humans) have been proposed as early pain-specific processing regions, and have been linked to subjective recognition of pain (Maihofner et al., 2006; Peyron et al., 2002; Strigo et al., 2005; Timmermann et al., 2001; Treede et al., 2000), encoding of pain intensity (Petrovic et al., 2000; Peyron et al., 1999; Timmermann et al., 2001), learning and memory of pain-related events (Dong et al., 1994; Ploner et al., 1999; Treede et al., 2000), and possibly the generation and maintenance of chronic pain states in humans ((Coghill et al., 1999; Coghill et al., 1994; Derbyshire et al., 1997; Gelnar et al., 1998; Greenspan et al., 1999; Kim et al., 2007; Mazzola et al., 2006;

Meyer et al., 1991; Morrow and Casey, 1992; Talbot et al., 1991; Torquati et al., 2002); for reviews, see (Apkarian et al., 2005; Treede et al., 2000)). PIns, as a part of the broadly defined operculoinsular region, has also been implicated as a pain-specific cortical region, even though its role remains debatable due to the lack of specificity of fMRI signals (Davis et al., 2015; Segerdahl et al., 2015). Although the rsFC networks of the insula and its subdivisions (i.e., anterior, middle and posterior pIns) have been explored in humans (Cauda et al., 2011; Deen et al., 2011; Taylor et al., 2009), its specific relationship to the S2 pain network have not been fully explored. Partially due to their close proximity along the *Sylvian fissure*, S2 and pIns regions are usually hard to separate with high confidence using functional signals. One unique advantage of studying the nociceptive processing circuits of S2 and pIns in monkeys is that the definition of cortical regions is based on not only the cytoarchitectonic features of the tissue, but also on anatomical and functional connections, as well as neuronal response features. We do not think the strong S2-pIns connection resulted from their close spatial proximity for the following two reasons. First, our previous rsfMRI studies of local meso-scale cortical networks have demonstrated that the strength of the inter-regional rsFC is determined primarily by their functional similarity, not their spatial proximity. For example, our previous resting state fMRI study of S1 sub-regions have shown that, even though the distance between digit regions area 3a and 1 is two times larger than that between areas 3b and 1, their rsFC strengths were comparable (Wang et al., 2013). Second, the two stimulus-evoked activation peaks (Fig. 1C) and local rsFC profiles (Figs. 2C–D) in S2 and pIns regions are clearly separable, indicating that the resolution at 9.4T used in this study is adequate for differentiating these two functionally distinct regions. We think the increased fMRI signal- and contrast-noise ratios allowed us to functionally localize S2 and pIns regions in monkeys, and then map their rsFC networks with improved spatial precision.

One novel finding of the present study is the identification of two distinct and hierarchically organized functional circuits of S2 and pIns, based on the strength of resting state inter-regional functional connectivity. Our lab and others have demonstrated that rsfMRI signals are robust and reliable in identifying and parcellating functional connectivity networks in anesthetized monkeys (Hutchison et al., 2013; Shmuel and Leopold, 2008; Vincent et al., 2007; Wang et al., 2013). By taking advantage of the high signal- and contrast-noise ratios of rsMRI signals at 9.4T, we successfully parcellated the intrinsic networks of S2 and pIns nociceptive regions by selecting the seed regions that responded to nociceptive heat stimuli in each individual subject. This approach is effective, because it permits reliable identification of nociceptive processing regions and reduction of inter-subject variability. Importantly, our spatial similarity and overlap analyses of rsFC maps support the existence of two distinct intrinsic functional circuits with minor overlap (~7%): S2-S1-area 7b and pIns-ACC-PCC. Building upon the known functions of these regions in the representation of pain, we propose that S2-pIns serves as a hub that connects sensory and affective nociceptive networks.

### 4.3. High spatial correspondence between nociceptive activation and rsFC networks of S2 and pIns regions

Another interesting finding of this study is the high degree of spatial similarity and overlap between the combined rsFC map of S2/pIns and the nociceptive heat activation map in the whole brain of monkeys. This finding is consistent with our previous observations within S1 cortex, and supports the notion that cortical regions engaged in the same function (e.g., nociceptive input processing) are intrinsically connected at rest. The observation of significantly increased overlap between the combined S2-pIns/rsFC network and activation map (Fig. 4B) supports that the networks of S2-rsFC are fairly independent, so the shared overlap region among all three maps is small/partial. We showed here again that rsFC is a powerful measure for probing intrinsic functional circuits within the central nervous system (Biswal et al., 1995; van den Heuvel and Pol, 2010). To our knowledge, our observation is the first demonstration of close spatial correspondence between combined rsFC networks of S2/pIns and the nociceptive heat processing networks in the non-human primate brain. The core network includes sub-regions of S1, S2, area 7b, pIns, and ACC. PCC is the only region shown to be part of S2-pIns rsFC network, but not a part of the information processing network (i.e., heat activation map). In humans, pIns has also been shown to exhibit strong rsFC to S1 and S2 cortices (Wiech et al., 2014). Although the emerging evidence supports the engagement of area 7b (part of inferior parietal cortex in primates) in nociception, the specific function of area 7b and its position within the S2-pIns networks need to be further explored with invasive means. We now have ongoing fMRI-guided microelectrode recording studies aiming to further explore the specific information encoding functions of these lateral sulcus regions and the underlying neural electrophysiological basis of the S2-pIns rsFC signals. Together, the present study has confirmed and extended our previous finding of refined tactile and nociceptive processing within S1 cortex (Chen et al., 2012; Chen et al., 2001; Chen et al., 2007) into the whole-brain nociception network. The high correspondence between stimulus-evoked and rsFC patterns underscores the potentials of using rsfMRI signals to parcellate functionally specific brain circuits. In summary, our findings of strong S2-pIns functional connection are aligned well with the observation in humans using the same rsfMRI signals (Wiech et al., 2014). Delineation of these two fine-scale functional circuits has refined the understanding of nociceptive processing networks in primates, and will form the functional network foundation for future investigations to understand the specific functions of each network in both animals and humans.

### 4.4. Implications of nociceptive heat evoked fMRI signals changes in ACC and PF cortices in anesthetized monkeys

ACC and PF engage in human pain perception. ACC is linked to the affective processing of pain, and also likely serves as an important relay station in descending inhibitory control of pain (Bingel et al., 2006; Lieberman and Eisenberger, 2015; Qu et al., 2011; Rainville et al., 1997; Rance et al., 2014; Russo and Sheth, 2015). PF has been proposed as a modulatory area for pain (Hardy and Haigler, 1985; Jahn et al., 2016; Lorenz et al., 2003; Nardone et al., 2017; Wiech et al., 2006). Nevertheless, detection of nociceptive heat-evoked fMRI signal changes in these two cortices (ACC and PF), as well as their robust functional connections to the pIns region under anesthesia, further supports their fundamental roles in nociceptive information processing without consciousness. Activity captured by fMRI signals likely

reflects the basic neurobiology processes that eventually lead to conscious pain perception in alert subjects. Studies have shown that introduction of anesthesia does not abolish neural electricity, but rather predominantly alters the frequency compositions of the electrical signals and reduces the integration and synchrony of electrical activity (Breshears et al., 2010; Hudetz, 2012; Shulman et al., 2009). The synchronized low frequency fMRI signal fluctuations in these high order brain regions could very likely relate to the baseline spontaneous neuronal activity that are known to consume energy (Hutchison et al., 2013; Liang et al., 2012; Shulman et al., 2009). Building upon this evidence, we believe our findings are not products of physiological noise, and we attribute our findings to the utilization of light isoflurane anesthesia and careful maintenance of physiological condition to reduce signal variation during fMRI data acquisition. We believe the significantly increased fMRI signal-noise ratio permitted reliable detection of stimulus-evoked activation at the individual subject level. We have shown previously that fMRI and neuronal electrophysiological signals remained robust under the operation range of 0.8–1.2% isoflurane in our experiments (Chen et al., 2011; Chen et al., 2007; Wang et al., 2013; Zhang et al., 2007). Nevertheless, the directions of information flow and neuronal response features of heat-evoked fMRI signal changes, as well as the signal fluctuations of the rsfMRI signals in these regions, remain to be further established.

## 5. Conclusions

Similar to the observations in human fMRI studies, we detected heat nociceptive stimuli-related fMRI activation in widespread brain regions bilaterally. Subsequent seed-based resting-state functional connectivity analysis identified two distinct and hierarchically organized nociceptive rsFC networks that are joined by the S2-pIns connection. The rsFC networks of S2 and pIns exhibited limited overlap, but their combined rsFC networks corresponded very well with nociceptive heat-evoked activation maps.

## Acknowledgements

This study is supported by a Dana Foundation and a National Institutes of Health Grant R01 NS069909 to L.M.C. We thank Chaohui Tang for her technical support on animal preparation, Fuxue Xin for his assistance on fMRI data collection, and George Wilson III for language editing of the manuscript.

## Abbreviations:

| | |
|---|---|
| **(ACC)** | Anterior cingulate cortex |
| **(Aud)** | auditory cortex |
| **(HRF)** | hemodynamic response function |
| **(Pari)** | parietal cortex |
| **(PCC)** | posterior cingulate cortex |
| **(pIns)** | posterior insula cortices |
| **(PF)** | prefrontal cortex |

| | |
|---|---|
| **(M1)** | primary motor cortex |
| **(S1)** | primary somatosensory cortex |
| **(rsfMRI)** | resting-state fMRI |
| **(rsFC)** | resting-state functional connectivity |
| **(S2)** | secondary somatosensory cortex |
| **(SCC)** | spatial correlation coefficient |
| **(SMA)** | supplementary motor area |

## References


Apkarian AV, Bushnell MC, Treede RD, Zubieta JK, 2005 Human brain mechanisms of pain perception and regulation in health and disease. Eur J Pain 9, 463–484. [PubMed: 15979027]

Apkarian AV, Thomas PS, Krauss BR, Szeverenyi NM, 2001 Prefrontal cortical hyperactivity in patients with sympathetically mediated chronic pain. Neurosci Lett 311, 193–197. [PubMed: 11578827]

Baliki MN, 2009 Parsing Pain Perception Between Nociceptive Representation and Magnitude Estimation. J Neurophysiol 101, 875–887. [PubMed: 19073802]

Baliki MN, Geha PY, Apkarian AV, Chialvo DR, 2008 Beyond feeling: Chronic pain hurts the brain, disrupting the default-mode network dynamics. J Neurosci 28, 1398–1403. [PubMed: 18256259]

Bamiou DE, Musiek FE, Luxon LM, 2003 The insula (Island of Reil) and its role in auditory processing. Brain Res Brain Res Rev 42, 143–154. [PubMed: 12738055]

Bingel U, Lorenz J, Schoell E, Weiller C, Buchel C, 2006 Mechanisms of placebo analgesia: rACC recruitment of a subcortical antinociceptive network. Pain 120, 8–15. [PubMed: 16364549]

Biswal B, Yetkin FZ, Haughton VM, Hyde JS, 1995 Functional Connectivity in the Motor Cortex of Resting Human Brain Using Echo-Planar Mri. Magn Reson Med 34, 537–541. [PubMed: 8524021]

Bornhovd K, Quante M, Glauche V, Bromm B, Weiller C, Buchel C, 2002 Painful stimuli evoke different stimulus-response functions in the amygdala, prefrontal, insula and somatosensory cortex: a single-trial fMRI study. Brain 125, 1326–1336. [PubMed: 12023321]

Breshears JD, Roland JL, Sharma M, Gaona CM, Freudenburg ZV, Tempelhoff R, Avidan MS, Leuthardt EC, 2010 Stable and dynamic cortical electrophysiology of induction and emergence with propofol anesthesia. Proc Natl Acad Sci U S A 107, 21170–21175. [PubMed: 21078987]

Casey KL, 1999 Forebrain mechanisms of nociception and pain: analysis through imaging. Proc Natl Acad Sci U S A 96, 7668–7674. [PubMed: 10393878]

Cauda F, D'Agata F, Sacco K, Duca S, Geminiani G, Vercelli A, 2011 Functional connectivity of the insula in the resting brain. Neuroimage 55, 8–23. [PubMed: 21111053]

Chen ACN, 2001 New perspectives in EEG/MEG brain mapping and PET/fMRI neuroimaging of human pain. Int J Psychophysiol 42, 147–159. [PubMed: 11587773]

Chen LM, Dillenburger BC, Wang F, Friedman RM, Avison MJ, 2011 High-resolution functional magnetic resonance imaging mapping of noxious heat and tactile activations along the central sulcus in New World monkeys. Pain 152, 522–532. [PubMed: 21177033]

Chen LM, Dillenburger BC, Wang F, Tang CH, 2012 Differential fMRI activation to noxious heat and tactile stimuli in parasylvian areas of new world monkeys. Pain 153, 158–169. [PubMed: 22115923]

Chen LM, Turner GH, Friedman RM, Zhang N, Gore JC, Roe AW, Avison MJ, 2007 High-resolution maps of real and illusory tactile activation in primary somatosensory cortex in individual monkeys with functional magnetic resonance imaging and optical imaging. J Neurosci 27, 9181–9191. [PubMed: 17715354]

Chudler EH, Dong WK, Kawakami Y, 1986 Cortical nociceptive responses and behavioral correlates in the monkey. Brain Res 397, 47–60. [PubMed: 3801865]

Coghill RC, Sang CN, Maisog JM, Iadarola MJ, 1999 Pain intensity processing within the human brain: a bilateral, distributed mechanism. J Neurophysiol 82, 1934–1943. [PubMed: 10515983]

Coghill RC, Talbot JD, Evans AC, Meyer E, Gjedde A, Bushnell MC, Duncan GH, 1994 Distributed processing of pain and vibration by the human brain. J Neurosci 14, 4095–4108. [PubMed: 8027764]

Coq JO, Qi H, Collins CE, Kaas JH, 2004 Anatomical and functional organization of somatosensory areas of the lateral fissure of the New World titi monkey (Callicebus moloch). J Comp Neurol 476, 363–387. [PubMed: 15282711]

Davis KD, Bushnell MC, Iannetti GD, St Lawrence K, Coghill R, 2015 Evidence against pain specificity in the dorsal posterior insula. F1000Res 4, 362. [PubMed: 26401267]

Davis KD, Moayedi M, 2013 Central Mechanisms of Pain Revealed Through Functional and Structural MRI. J Neuroimmune Pharmacol 8, 518–534. [PubMed: 22825710]

Deen B, Pitskel NB, Pelphrey KA, 2011 Three systems of insular functional connectivity identified with cluster analysis. Cereb Cortex 21, 1498–1506. [PubMed: 21097516]

Derbyshire SW, Jones AK, Gyulai F, Clark S, Townsend D, Firestone LL, 1997 Pain processing during three levels of noxious stimulation produces differential patterns of central activity. Pain 73, 431–445. [PubMed: 9469535]

Dong WK, Chudler EH, Sugiyama K, Roberts VJ, Hayashi T, 1994 Somatosensory, multisensory, and task-related neurons in cortical area 7b (PF) of unanesthetized monkeys. J Neurophysiol 72, 542–564. [PubMed: 7983518]

Dong WK, Hayashi T, Roberts VJ, Fusco BM, Chudler EH, 1996 Behavioral outcome of posterior parietal cortex injury in the monkey. Pain 64, 579–587. [PubMed: 8783324]

Edelbrock C, McLaughlin B, 1980 Hierarchical cluster analysis using intraclass correlations: A mixture model study. Multivariate Behav Res 15, 299–318. [PubMed: 26794184]

Fox MD, Greicius M, 2010 Clinical applications of resting state functional connectivity. Front Syst Neurosci 4, 19. [PubMed: 20592951]

Frot M, Magnin M, Mauguiere F, Garcia-Larrea L, 2013 Cortical representation of pain in primary sensory-motor areas (S1/M1)-a study using intracortical recordings in humans. Hum Brain Mapp 34, 2655–2668. [PubMed: 22706963]

Garcia-Larrea L, Frot M, Valeriani M, 2003 Brain generators of laser-evoked potentials: from dipoles to functional significance. Neurophysiol Clin 33, 279–292. [PubMed: 14678842]

Gelnar PA, Krauss BR, Szeverenyi NM, Apkarian AV, 1998 Fingertip representation in the human somatosensory cortex: an fMRI study. Neuroimage 7, 261–283. [PubMed: 9626668]

Gergen JA, MacLean PD, 1962 A stereotaxic atlas of the squirrel monkey's brain (Saimiri sciureus).

Glover GH, Li TQ, Ress D, 2000 Image-based method for retrospective correction of physiological motion effects in fMRI: RETROICOR. Magn Reson Med 44, 162–167. [PubMed: 10893535]

Greenspan JD, Lee RR, Lenz FA, 1999 Pain sensitivity alterations as a function of lesion location in the parasylvian cortex. Pain 81, 273–282. [PubMed: 10431714]

Greicius MD, Krasnow B, Reiss AL, Menon V, 2003 Functional connectivity in the resting brain: A network analysis of the default mode hypothesis. Proc Natl Acad Sci U S A 100, 253–258. [PubMed: 12506194]

Haefeli J, Freund P, Kramer JLK, Blum J, Luechinger R, Curt A, 2014 Differences in Cortical Coding of Heat Evoked Pain Beyond the Perceived Intensity: An fMRI and EEG Study. Hum Brain Mapp 35, 1379–1389. [PubMed: 23450833]

Hardy SGP, Haigler HJ, 1985 Prefrontal Influences Upon the Midbrain - a Possible Route for Pain Modulation. Brain Res 339, 285–293. [PubMed: 4027627]

Hudetz AG, 2012 General anesthesia and human brain connectivity. Brain Connect 2, 291–302. [PubMed: 23153273]

Hutchison RM, Womelsdorf T, Gati JS, Everling S, Menon RS, 2013 Resting-state networks show dynamic functional connectivity in awake humans and anesthetized macaques. Hum Brain Mapp 34, 2154–2177. [PubMed: 22438275]

Iannetti GD, Zambreanu L, Cruccu G, Tracey I, 2005 Operculoinsular cortex encodes pain intensity at the earliest stages of cortical processing as indicated by amplitude of laser-evoked potentials in humans. Neuroscience 131, 199–208. [PubMed: 15680703]

Jahn A, Nee DE, Alexander WH, Brown JW, 2016 Distinct Regions within Medial Prefrontal Cortex Process Pain and Cognition. J Neurosci 36, 12385–12392. [PubMed: 27807031]

Johnson SC, 1967 Hierarchical clustering schemes. Psychometrika 32, 241–254. [PubMed: 5234703]

Jones EG, Burton H, 1976 Areal differences in the laminar distribution of thalamic afferents in cortical fields of the insular, parietal and temporal regions of primates. J Comp Neurol 168, 197–247. [PubMed: 821974]

Kaskan PM, Lu HD, Dillenburger BC, Roe AW, Kaas JH, 2007 Intrinsic-signal optical imaging reveals cryptic ocular dominance columns in primary visual cortex of New World owl monkeys. Front Neurosci 1, 67–75. [PubMed: 18974855]

Kim JH, Greenspan JD, Coghill RC, Ohara S, Lenz FA, 2007 Lesions limited to the human thalamic principal somatosensory nucleus (ventral caudal) are associated with loss of cold sensations and central pain. J Neurosci 27, 4995–5004. [PubMed: 17475808]

Koyama T, Kato K, Tanaka YZ, Mikami A, 2001 Anterior cingulate activity during pain-avoidance and reward tasks in monkeys. Neurosci Res 39, 421–430. [PubMed: 11274741]

Koyama T, Tanaka YZ, Mikami A, 1998 Nociceptive neurons in the macaque anterior cingulate activate during anticipation of pain. Neuroreport 9, 2663–2667. [PubMed: 9721952]

Kwan CL, Crawley AP, Mikulis DJ, Davis KD, 2000 An fMRI study of the anterior cingulate cortex and surrounding medial wall activations evoked by noxious cutaneous heat and cold stimuli. Pain 85, 359–374. [PubMed: 10781909]

Liang Z, King J, Zhang N, 2012 Intrinsic organization of the anesthetized brain. J Neurosci 32, 10183–10191. [PubMed: 22836253]

Lieberman MD, Eisenberger NI, 2015 The dorsal anterior cingulate cortex is selective for pain: Results from large-scale reverse inference. Proc Natl Acad Sci U S A 112, 15250–15255. [PubMed: 26582792]

Lorenz J, Minoshima S, Casey KL, 2003 Keeping pain out of mind: the role of the dorsolateral prefrontal cortex in pain modulation. Brain 126, 1079–1091. [PubMed: 12690048]

Maihofner C, Herzner B, Otto Handwerker H, 2006 Secondary somatosensory cortex is important for the sensory-discriminative dimension of pain: a functional MRI study. Eur J Neurosci 23, 1377–1383. [PubMed: 16553798]

Malinen S, Vartiainena N, Hlushchuk Y, Koskinen M, Ramkumar P, Forss N, Kalso E, Hari R, 2010 Aberrant temporal and spatial brain activity during rest in patients with chronic pain. Proc Natl Acad Sci U S A 107, 6493–6497. [PubMed: 20308545]

Margulies DS, Vincent JL, Kelly C, Lohmann G, Uddin LQ, Biswal BB, Villringer A, Castellanos FX, Milham MP, Petrides M, 2009 Precuneus shares intrinsic functional architecture in humans and monkeys. Proc Natl Acad Sci U S A 106, 20069–20074. [PubMed: 19903877]

May A, 2008 Chronic pain may change the structure of the brain. Pain 137, 7–15. [PubMed: 18410991]

Mazzola L, Isnard J, Mauguiere F, 2006 Somatosensory and pain responses to stimulation of the second somatosensory area (SII) in humans. A comparison with SI and insular responses. Cereb Cortex 16, 960–968. [PubMed: 16177270]

Meyer RA, Davis KD, Cohen RH, Treede RD, Campbell JN, 1991 Mechanically insensitive afferents (MIAs) in cutaneous nerves of monkey. Brain Res 561, 252–261. [PubMed: 1802341]

Morrow TJ, Casey KL, 1992 State-related modulation of thalamic somatosensory responses in the awake monkey. J Neurophysiol 67, 305–317. [PubMed: 1569463]

Napadow V, LaCount L, Park K, As-Sanie S, Clauw DJ, Harris RE, 2010 Intrinsic Brain Connectivity in Fibromyalgia Is Associated With Chronic Pain Intensity. Arthritis Rheum 62, 2545–2555. [PubMed: 20506181]

Nardone R, Holler Y, Langthaler PB, Lochner P, Golaszewski S, Schwenker K, Brigo F, Trinka E, 2017 rTMS of the prefrontal cortex has analgesic effects on neuropathic pain in subjects with spinal cord injury. Spinal Cord 55, 20–25. [PubMed: 27241450]

Oshiro Y, Quevedo AS, McHaffie JG, Kraft RA, Coghill RC, 2007 Brain mechanisms supporting spatial discrimination of pain. J Neurosci 27, 3388–3394. [PubMed: 17392455]

Pavlides C, Miyashita E, Asanuma H, 1993 Projection from the sensory to the motor cortex is important in learning motor skills in the monkey. J Neurophysiol 70, 733–741. [PubMed: 8410169]

Petrof I, Viaene AN, Sherman SM, 2015 Properties of the primary somatosensory cortex projection to the primary motor cortex in the mouse. J Neurophysiol 113, 2400–2407. [PubMed: 25632081]

Petrovic P, Petersson KM, Ghatan PH, Stone-Elander S, Ingvar M, 2000 Pain-related cerebral activation is altered by a distracting cognitive task. Pain 85, 19–30. [PubMed: 10692599]

Peyron R, Frot M, Schneider F, Garcia-Larrea L, Mertens P, Barral FG, Sindou M, Laurent B, Mauguiere F, 2002 Role of operculoinsular cortices in human pain processing: converging evidence from PET, fMRI, dipole modeling, and intracerebral recordings of evoked potentials. Neuroimage 17, 1336–1346. [PubMed: 12414273]

Peyron R, Garcia-Larrea L, Gregoire MC, Costes N, Convers P, Lavenne F, Mauguiere F, Michel D, Laurent B, 1999 Haemodynamic brain responses to acute pain in humans: sensory and attentional networks. Brain 122, 1765–1780. [PubMed: 10468515]

Peyron R, Laurent B, Garcia-Larrea L, 2000 Functional imaging of brain responses to pain. A review and meta-analysis (2000). Neurophysiol Clin 30, 263–288. [PubMed: 11126640]

Ploner M, Freund HJ, Schnitzler A, 1999 Pain affect without pain sensation in a patient with a postcentral lesion. Pain 81, 211–214. [PubMed: 10353510]

Price DD, 2000 Psychological and neural mechanisms of the affective dimension of pain. Science 288,1769–1772. [PubMed: 10846154]

Qu C, King T, Okun A, Lai J, Fields HL, Porreca F, 2011 Lesion of the rostral anterior cingulate cortex eliminates the aversiveness of spontaneous neuropathic pain following partial or complete axotomy. Pain 152, 1641–1648. [PubMed: 21474245]

Rainville P, Duncan GH, Price DD, Carrier B, Bushnell MC, 1997 Pain affect encoded in human anterior cingulate but not somatosensory cortex. Science 277, 968–971. [PubMed: 9252330]

Ramsden BM, Hung CP, Roe AW, 2001 Real and illusory contour processing in area V1 of the primate: a cortical balancing act. Cereb Cortex 11, 648–665. [PubMed: 11415967]

Rance M, Ruttorf M, Nees F, Schad LR, Flor H, 2014 Real time fMRI feedback of the anterior cingulate and posterior insular cortex in the processing of pain. Hum Brain Mapp 35, 5784–5798. [PubMed: 25045017]

Renier LA, Anurova I, De Volder AG, Carlson S, VanMeter J, Rauschecker JP, 2009 Multisensory integration of sounds and vibrotactile stimuli in processing streams for “what” and “where”. J Neurosci 29, 10950–10960. [PubMed: 19726653]

Rodgers KM, Benison AM, Klein A, Barth DS, 2008 Auditory, somatosensory, and multisensory insular cortex in the rat. Cereb Cortex 18, 2941–2951. [PubMed: 18424777]

Russo JF, Sheth SA, 2015 Deep brain stimulation of the dorsal anterior cingulate cortex for the treatment of chronic neuropathic pain. Neurosurg Focus 38, E11.

Saleem KS, Logothetis NK, 2012 A combined MRI and histology atlas of the rhesus monkey brain in stereotaxic coordinates. Academic Press.

Sawamoto N, Honda M, Okada T, Hanakawa T, Kanda M, Fukuyama H, Konishi J, Shibasaki H, 2000 Expectation of pain enhances responses to nonpainful somatosensory stimulation in the anterior cingulate cortex and parietal operculum/posterior insula: an event-related functional magnetic resonance imaging study. J Neurosci 20, 7438–7445. [PubMed: 11007903]

Scholvinck ML, Maier A, Ye FQ, Duyn JH, Leopold DA, 2010 Neural basis of global resting-state fMRI activity. Proc Natl Acad Sci U S A 107, 10238–10243. [PubMed: 20439733]

Segerdahl AR, Mezue M, Okell TW, Farrar JT, Tracey I, 2015 The dorsal posterior insula subserves a fundamental role in human pain. Nat Neurosci 18, 499–500. [PubMed: 25751532]

Shmuel A, Leopold DA, 2008 Neuronal correlates of spontaneous fluctuations in fMRI signals in monkey visual cortex: Implications for functional connectivity at rest. Hum Brain Mapp 29, 751–761. [PubMed: 18465799]

Shulman RG, Hyder F, Rothman DL, 2009 Baseline brain energy supports the state of consciousness. Proc Natl Acad Sci U S A 106, 11096–11101. [PubMed: 19549837]

Strigo IA, Albanese MC, Bushnell MC, Duncan GH, 2005 Visceral and cutaneous pain representation in parasylvian cortex. Neurosci Lett 384, 54–59. [PubMed: 15905031]

Talbot JD, Marrett S, Evans AC, Meyer E, Bushnell MC, Duncan GH, 1991 Multiple representations of pain in human cerebral cortex. Science 251, 1355–1358. [PubMed: 2003220]

Taylor KS, Seminowicz DA, Davis KD, 2009 Two systems of resting state connectivity between the insula and cingulate cortex. Hum Brain Mapp 30, 2731–2745. [PubMed: 19072897]

Timmermann L, Ploner M, Haucke K, Schmitz F, Baltissen R, Schnitzler A, 2001 Differential coding of pain intensity in the human primary and secondary somatosensory cortex. J Neurophysiol 86, 1499–1503. [PubMed: 11535693]

Torquati K, Pizzella V, Della Penna S, Franciotti R, Babiloni C, Rossini PM, Romani GL, 2002 Comparison between SI and SII responses as a function of stimulus intensity. Neuroreport 13, 813–819. [PubMed: 11997693]

Treede RD, Apkarian AV, Bromm B, Greenspan JD, Lenz FA, 2000 Cortical representation of pain: functional characterization of nociceptive areas near the lateral sulcus. Pain 87, 113–119. [PubMed: 10924804]

van den Heuvel MP, Pol HEH, 2010 Exploring the brain network: A review on resting-state fMRI functional connectivity. Eur Neuropsychopharmacol 20, 519–534. [PubMed: 20471808]

Vincent JL, Patel GH, Fox MD, Snyder AZ, Baker JT, Van Essen DC, Zempel JM, Snyder LH, Corbetta M, Raichle ME, 2007 Intrinsic functional architecture in the anaesthetized monkey brain. Nature 447, 83–U84. [PubMed: 17476267]

Vogel H, Port JD, Lenz FA, Solaiyappan M, Krauss G, Treede RD, 2003 Dipole source analysis of laser-evoked subdural potentials recorded from parasylvian cortex in humans. J Neurophysiol 89, 3051–3060. [PubMed: 12783950]

Wang Z, Chen LM, Negyessy L, Friedman RM, Mishra A, Gore JC, Roe AW, 2013 The Relationship of Anatomical and Functional Connectivity to Resting-State Connectivity in Primate Somatosensory Cortex. Neuron 78, 1116–1126. [PubMed: 23791200]

Wiech K, Jbabdi S, Lin CS, Andersson J, Tracey I, 2014 Differential structural and resting state connectivity between insular subdivisions and other pain-related brain regions. Pain 155, 2047–2055. [PubMed: 25047781]

Wiech K, Kalisch R, Weiskopf N, Pleger B, Stephan KE, Dolan RJ, 2006 Anterolateral prefrontal cortex mediates the analgesic effect of expected and perceived control over pain. J Neurosci 26, 11501–11509. [PubMed: 17079679]

Xu F, Liu N, Kida I, Rothman DL, Hyder F, Shepherd GM, 2003 Odor maps of aldehydes and esters revealed by functional MRI in the glomerular layer of the mouse olfactory bulb. Proc Natl Acad Sci U S A 100, 11029–11034. [PubMed: 12963819]

Zhang N, Gore JC, Chen LM, Avison MJ, 2007 Dependence of BOLD signal change on tactile stimulus intensity in SI of primates. Magn Reson Imaging 25, 784–794. [PubMed: 17614230]

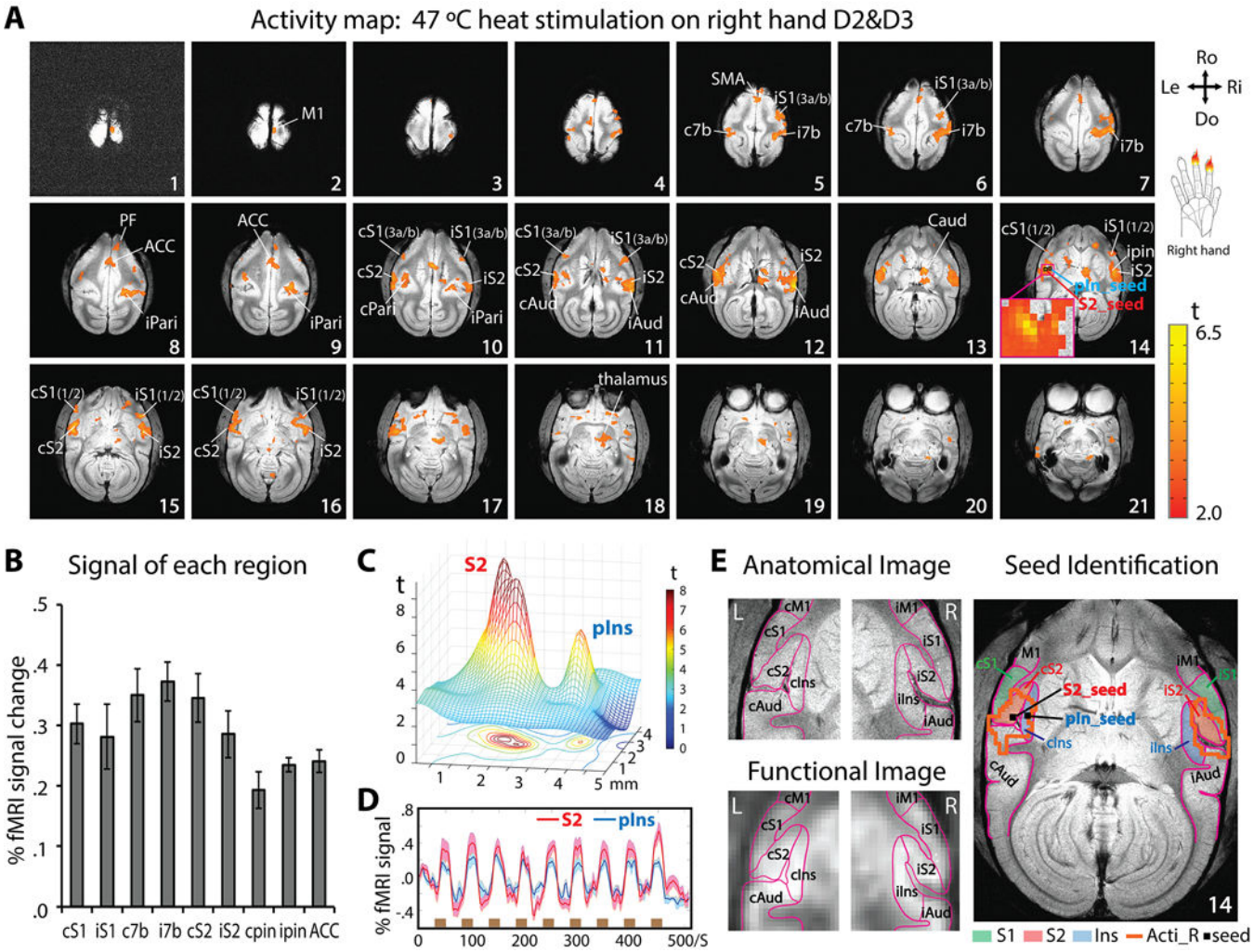


**Figure 1.**

Nociceptive heat-evoked fMRI activation maps from one representative squirrel monkey (SM-HAZ, session 1) and illustration of seeds identification for resting-state fMRI analysis. (A) Twenty-one axial images, sampled from top to bottom of the brain, show fMRI activations to 47 °C heat stimulation of right-hand D2 and D3 distal and middle phalanx. Slice 14 shows the selection of S2 (red arrow) and pIns (blue arrow) activation regions as seeds for subsequent rsFC analysis. The insert shows the enlarged view of two activation foci in S2 and pIns. Orientations (Ro: rostral, Do: dorsal, Ri: right, Le: left) and slice numbers are marked on the images. Color bar indicates the range of t values. (B) Group peak amplitudes of % BOLD signal changes (mean ± se) to 47 °C heat stimulation in different brain regions (n = 12 runs). (C) Mesh and contour plot of the activation profiles of the S2 and pIns region shown in the insert in slice 14 of A. (D) Time-courses of S2 (red line) and pIns (blue line) activations. The brown bars indicate stimulation blocks. (E) Top left image shows parcellated S2, pIns and surrounding regions based on an anatomical atlas (Gergen and MacLean, 1962, Saleem et al., 2012) overlaid on a structural MRI image. Bottom left image shows the corresponding outlines of parcellated regions overlaid on a functional EPI image. Right image illustrates the overlaid heat activation clusters in both hemispheres:

Acti-R (orange lines), S1, S2 and pIns regions (solid color patches) and the seeds in S2 and pIns (small black squares).

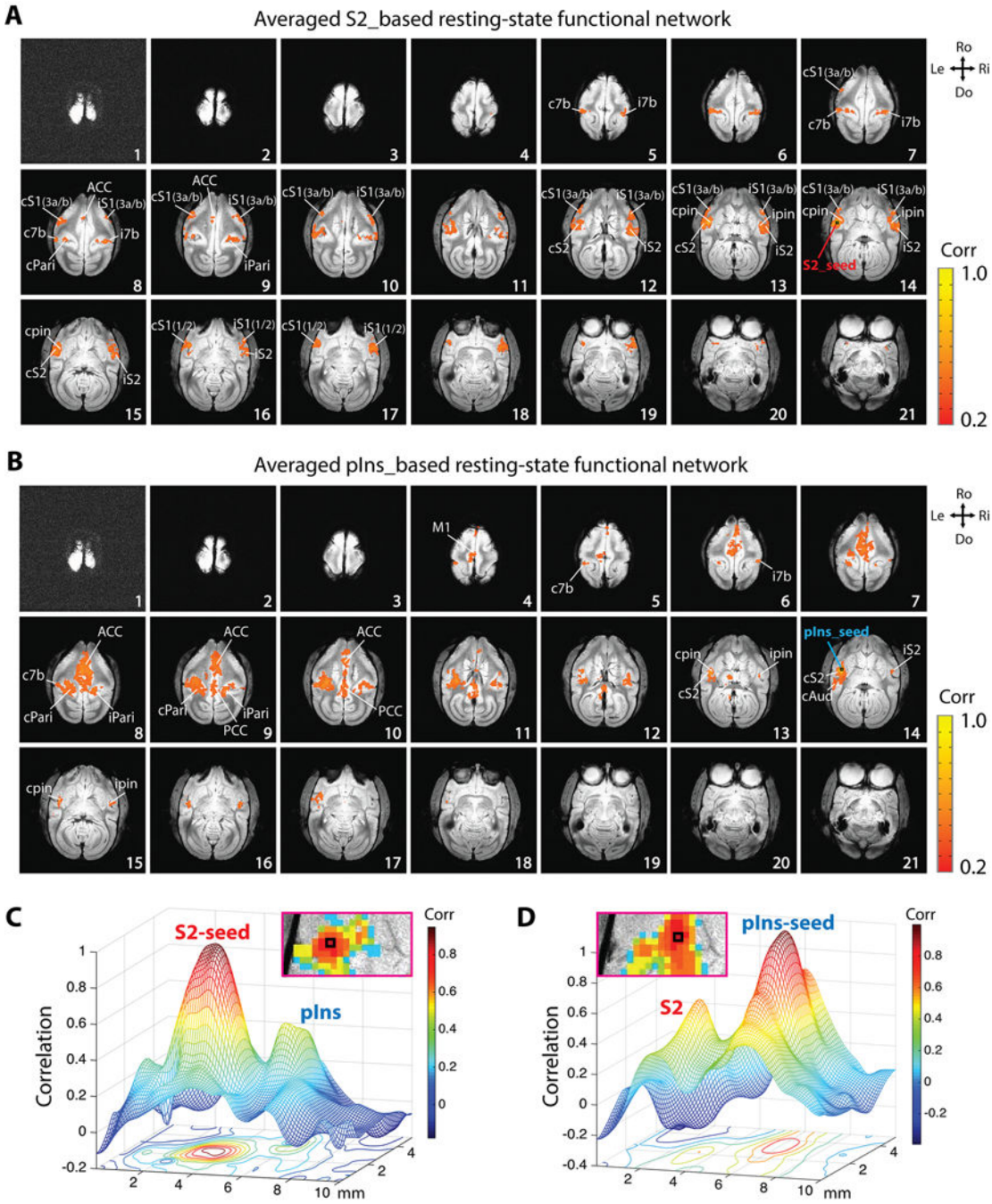


**Figure 2.**

Whole-brain resting-state functional connectivity (rsFC) maps of nociceptive pIns and S2 regions in the same representative session in Fig. 1. The seeds are chosen based on the nociceptive heat activation map in Fig. 1. (A) Whole-brain rsFC map of nociceptive S2 region. (B) Whole-brain rsFC map of nociceptive pIns region. S2 and pIns seeds are indicated by black boxes on slice 14. Correlation maps were computed from a total of 4 imaging runs (170 imaging volumes in each run). (C-D) Mesh and contour plot of local S2 and pIns correlation profiles in the S2-rsFC (C) and pIns-rsFC (D) map.

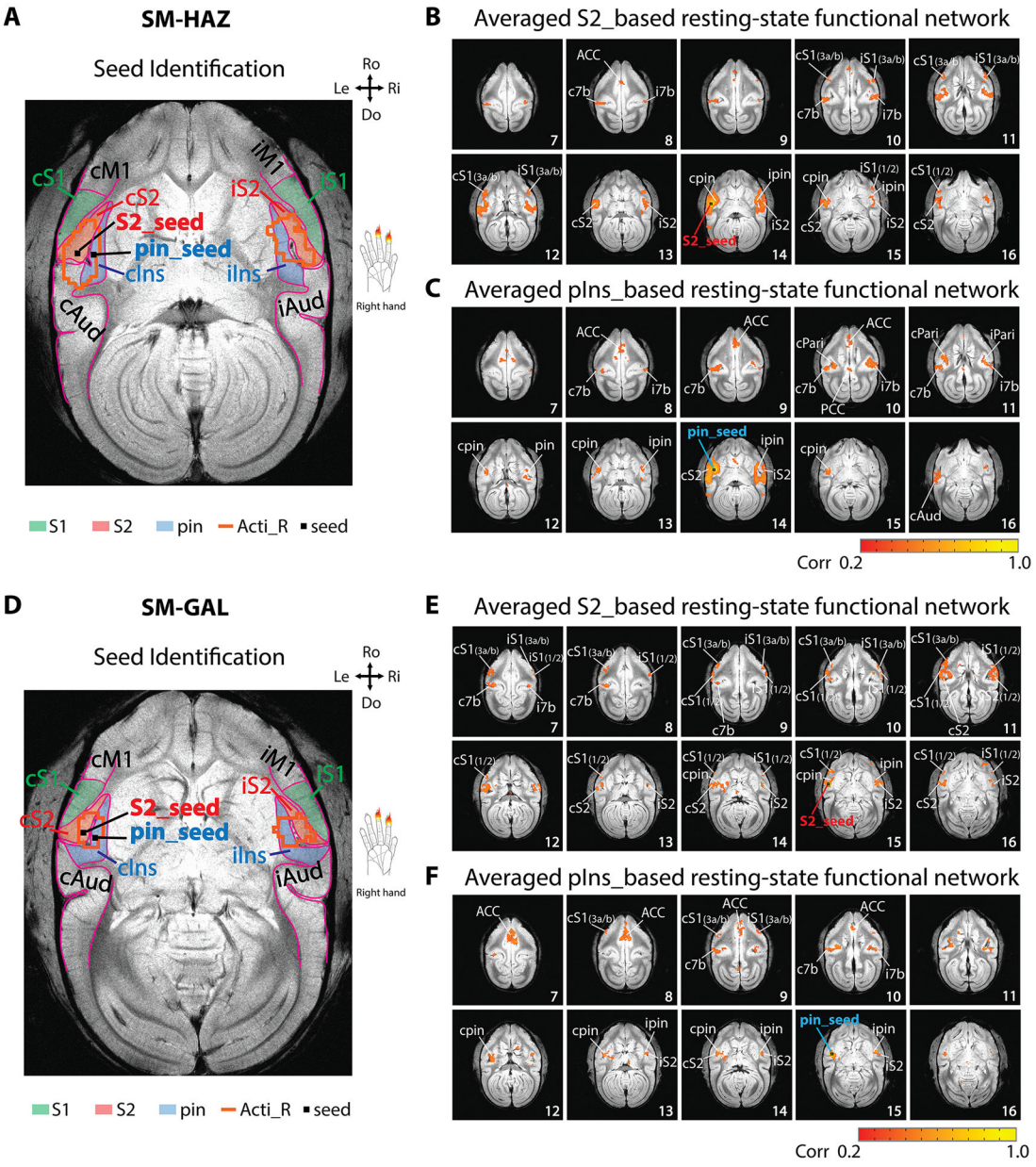


**Figure 3.**

Reproducibility of rsFC networks of nociceptive S2 and pIns regions in two other sessions (session 1 of SM-HAZ, SM-GAL). (A, D) S2 and pIns seeds identifications. (B, E) Whole-brain voxel-wise rsFC maps (correlation maps) of S2 seeds. (C, F) Whole-brain voxel-wise rsFC maps (correlation maps) of pIns seeds. N = 3 runs for SM-HAZ, and n = 4 runs for SM-GAL (170 volumes in each run). Color bars: range of correlation coefficient (r) values. Orientations are marked on the images (Ro: rostral, Do: dorsal, Ri: right, Le: left).

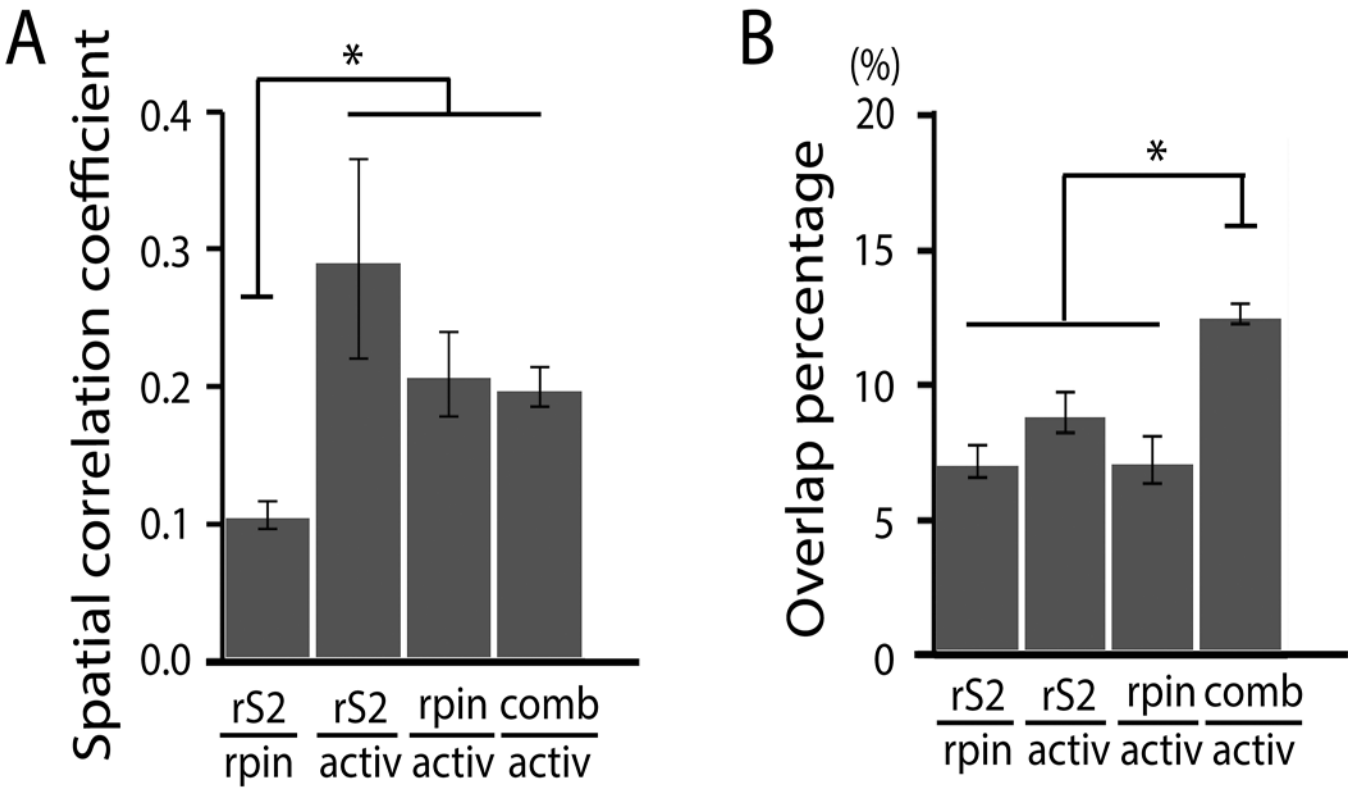


**Figure 4.**

Comparisons among nociceptive heat activation map, S2 rs-network, and pIns rs-network. (A) Spatial correlation coefficients between S2-based intrinsic map and pIns-based intrinsic map (rS2|rpin), S2-based intrinsic map and activation map (rS2|activ), pIns-based intrinsic map and activation map (rpin|activ), and combined intrinsic map and activity map (comb|activ). (B) Overlap percentages of rS2|rpin, rS2|activ, rpin|activ, and comb|activ. Number of S2 seeds = 10, number of pIns seeds = 12; Unpaired t-test, $*p < 0.05$, Error bars indicate standard error.

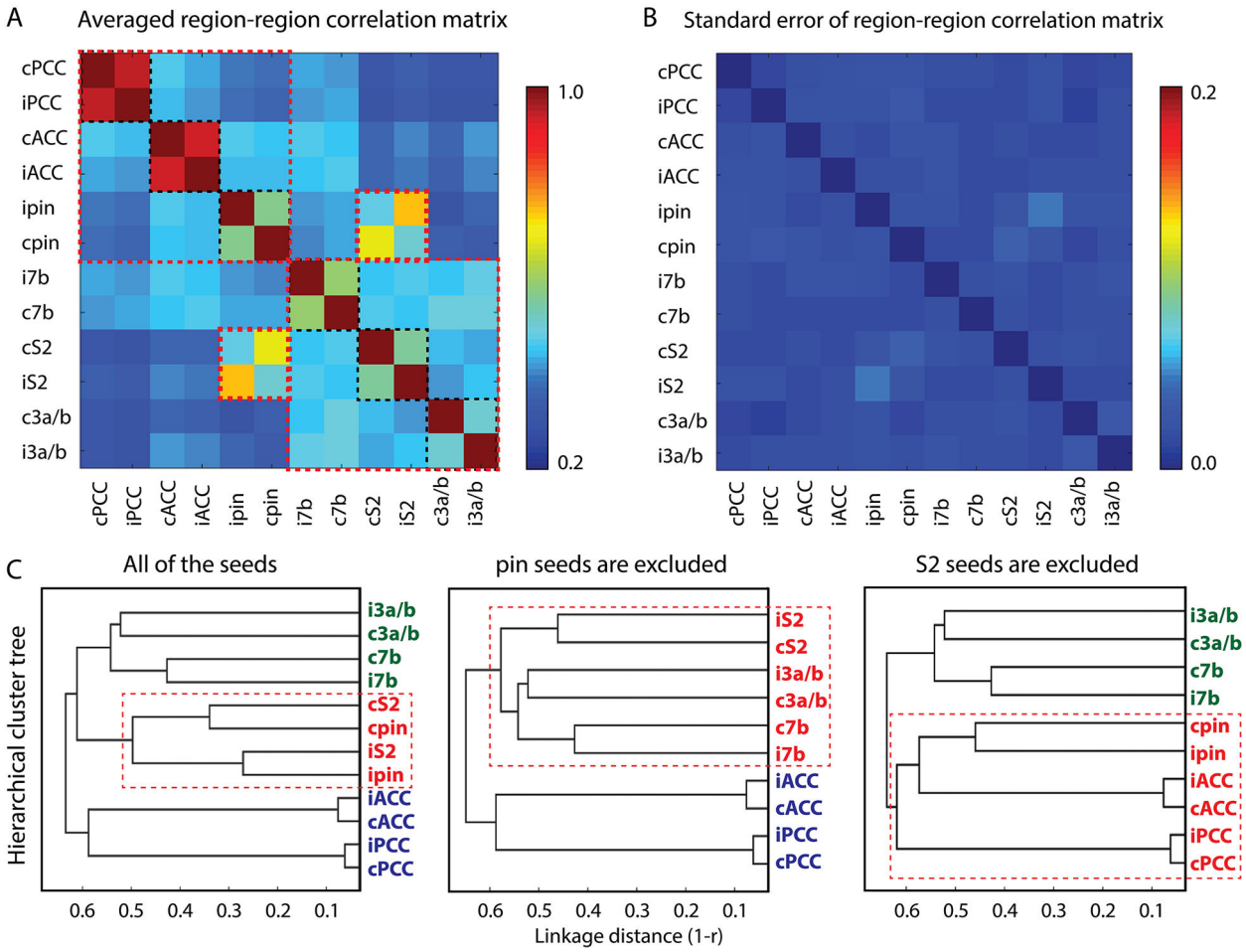


**Figure 5.**

Connectivity relationships among main regions identified in rsFC maps of nociceptive S2 and pIns region. (A) 2D matrix plot of the group averaged inter-regional correlation strength (*r*-value, see color bar for range). (B) 2D matrix plot of corresponding standard error in A. (C) Hierarchical cluster tree organization of connectivity strength rankings of all twelve seeds (left), ten seeds excluding ipsilateral and contralateral pIns (middle), and ten seeds excluding S2 ipsilateral and contralateral S2 (right). The x-axis indicates the distance (1-r) used for clustering with a weighted average-linkage algorithm (WPGMA). A total of 15 resting-state fMRI runs from 4 animals were included in the quantification.

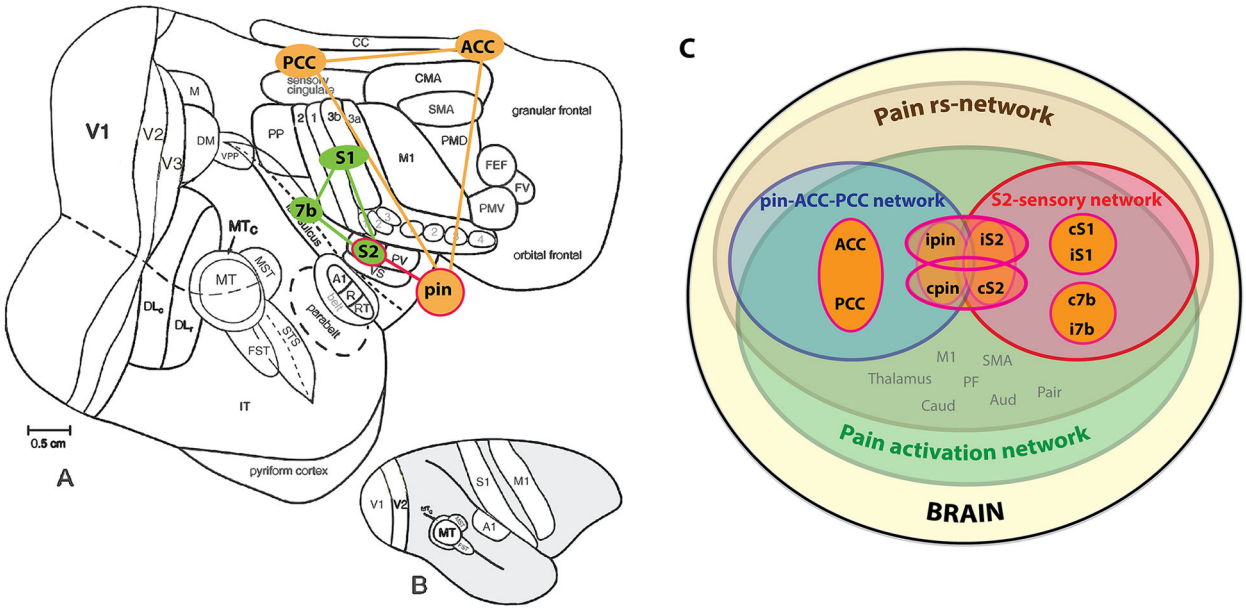


**Figure 6.**

Schematic summary of inter-region relationships in pain networks of squirrel monkeys. (A-B) Pain related-regions on a flattened view of the entire neocortex (A), and on a lateral view of the intact monkey brain (B). A-B modified from Kaskan et al., 2007. (C) Inter-region relationships in their rsFC strengths in pain rsFC networks of pIns and S2. S1 represents area 3a/3b.